# Three-dimensional development of cascade showers induced by 50-, 100-, and 300-GeV electrons

N. Hotta, H. Munakata, M. Sakata, and Y. Yamamoto
*Department of Physics, Konan University, Kobe, Japan*

S. Dake, H. Ito, and M. Miyanishi
*Department of Physics, Kobe University, Kobe, Japan*

K. Kasahara and T. Yuda
*Institute for Cosmic Ray Research, University of Tokyo, Tanashi, Japan*

K. Mizutani
*Department of Physics, Saitama University, Urawa, Japan*

I. Ohta
*Faculty of Education, Utsunomiya University, Utsunomiya, Japan*

(Received 17 December 1979)

Five emulsion chambers were analyzed with two different dilution factors exposed to the 50-, 100-, and 300-GeV electron beams at Fermi National Accelerator Laboratory. The longitudinal development and lateral distribution of the number of shower tracks within a certain radius ( $\leq 100\,\mu$m) both roughly agree with the theoretical transition and lateral curves by Nishimura and Kidd connected by a spacing factor equal to the dilution factor. The error of the cascade energy measurement by the conventional way, using the transition curves within a radius 50 $\mu$m, is 18–28 % for 50–100 GeV and 13–14 % for 300 GeV. Track length within a cylinder of the same radius gives less ambiguity than the above method, when the track length is summed up till the depth is greater than 1.4 times the depth of the maximum number of shower tracks within a radius 50 $\mu$m. Other results with details are also described.

## I. INTRODUCTION

The characteristic features of electromagnetic showers have been investigated with a variety of experimental techniques by using accelerator electron or photon beams at energies up to several ten GeV. In these studies, the following detectors, i.e., ionization chambers,[1] cloud chambers,[2] bubble chambers,[3] spark chambers,[4] scintillation counters[5] or probes,[6] photographic films,[7] and thermoluminescent dosimetry[8] were frequently employed as the needs of the case demanded.

On the other hand, of course, theoretical works have been extensively carried out by many authors[9,10] under the proper approximations (approximation A or B). In particular, the rapid progress of computer and Monte Carlo techniques has made it possible to calculate in great detail the cascade development in close touch with the real conditions,[11] and the results are widely applicable to the design of the total-absorption-type detector used in high-energy experiments.

For the cosmic-ray region, where the energy concerned is extremely high, an analytical treatment combining the shower theory under approximation B with the scattering theory can be applied to the analysis of cosmic-ray phenomena. In experiments with emulsion stacks[12] or emulsion chambers,[13] the reliability of the energy determination of incident electrons or photons is closely coupled with the behavior of cascade showers near the shower axis. In 1963, Nishimura and Kidd[14] first calculated the lateral structure functions near the shower axis by the core approximation as they say, and since then the emulsion-chamber experiments have been continued on the basis of their calculation.[13]

The applicability of the core approximation has not yet been critically checked by the experiment. But, before now, various tests have been indirectly done, for example, by the method applying a kinematical relation between two $\gamma$ rays from $\pi^0 \rightarrow 2\gamma$ decay to two cascade showers observed in an emulsion chamber exposed to cosmic rays,[15] where the cascade energies were estimated by use of the Nishimura-Kidd curve. Alternatively, the consistency between the cascade energy and initial energy deduced independently by the scattering method for cascade electrons[16] may be found.

Recently, the Fermilab 400-GeV proton synchrotron made possible a cascade-shower study using the secondarily generated monoenergetic electron beams at energies up to 300 GeV. Then we ex-

 

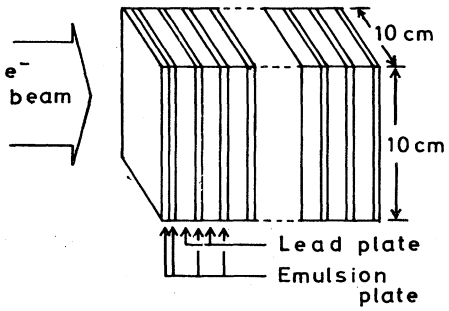


FIG. 1. Design of emulsion chamber.

posed our emulsion chambers to the beams for a study of the three-dimensional development near the shower axis.

In this paper the results of the analysis are compared with the theoretical calculation by Nishimura and Kidd.[10] The average transition curves and lateral distributions are described in Sec. IV, and also validity for the similarity relation is examined there. The fluctuation of the number of shower tracks or of the track length is described in Sec. V. The reliability of a conventional method of energy measurement[13] is discussed in Sec. VI.

## II. EXPERIMENTAL PROCEDURE

Our detector, i.e., emulsion chamber, is composed of nuclear emulsion plates and lead plates which are stacked alternately as schematically shown in Fig. 1. In this figure, nuclear emulsion 50 $\mu$m thick (Fuji ET7B) is coated on both sides of 800-$\mu$m-thick acryl base. The face area of each plate is 10 cm $\times$ 10 cm. A few emulsion plates at the top of the chamber are utilized to identify the incident particles. The emulsion chambers are specified by two dilution factors $d$ with different thickness of lead plates as given in Table I, where $d$ is defined by the ratio of the repeat distance of emulsion plate versus the thickness of a lead plate. In this paper are presented the results of analysis of five chambers with two different values of $d$, as summarized in Table II,

TABLE I. Dilution factor and thickness of the emulsion plate and lead plate.

| Dilution factor ($d$) | Lead plate (mm) | Acryl base ($\mu$m) | Emulsion ($\mu$m) |
|---|---|---|---|
| 1.18 | 5.0 | 800 | 50 + 50 |
| 1.36 | 2.5 | | |

exposed to 50-, 100-, and 300-GeV electron beams.

The electron beams with an energy resolution of $\pm \sim 2.0\%$[17] were irradiated at right angles to the central 64-cm$^2$ area of each chamber. The average densities of cascade events, found by microscopic scanning, are ~0.5 events/cm$^2$, ~2 events/cm$^2$, and ~1.5 events/cm$^2$ for the 50-, 100-, and 300-GeV beams, respectively.

Some cascade showers initiated by particles other than electrons were contaminated in this experiment. Among them, the photon-initiated showers are easily recognized by the lack of a corresponding single track in the top two nonshielded emulsion plates. Jet showers induced by $\pi^-$ mesons were found only in the chamber exposed to the 300-GeV beam. The jet showers can be also distinguished from the cascade showers by finding large-angle hadron tracks which penetrated the initial several plates, or by late start of shower in the lead plate of the chamber. In addition, there were some events accompanied by bremsstrahlung $\gamma$ rays which must have been emitted from the parent electron before arriving at the emulsion chamber. These events perhaps partly originated in the plastic scintillator located 30 cm in front of the emulsion chamber to confirm the passing of the electron beam and partly in the vacuum tube or in the air gap between the tube end and the emulsion chamber. All these contaminations, listed in Table III for each of the three energy incidences, were omitted from the analysis.

Moreover, we excluded some close events with mutual separation less than 800 $\mu$m for 300-GeV showers and less than 1500 $\mu$m for the 100-GeV

TABLE II. Construction of emulsion chamber and number of cascade events analyzed, No.

| Chamber | $d$ | Incident energy (GeV) | Emulsion (layers) | Total lead (cm) | Scanning depth (cm) | No. |
|---|---|---|---|---|---|---|
| C1 | 1.18 | 50 | 9 | 3.5 | 1.5 and 2.5 | 19 |
| C2 | 1.18 | 100 | 11 | 4.5 | 3.0 | 60 |
| C3 | 1.18 | 300 | 16 | 7.0 | 3.0 | 30 |
| A2 | 1.36 | 100 | 20 | 4.5 | 2.5 | 49 |
| A3 | 1.36 | 300 | 30 | 7.0 | 4.0 | 31 |

TABLE III. The number and rate of beam contamination.

| Incident energy (GeV) | Number (rate) of contamination $\gamma$ | $e^- + \gamma$ | $\pi^-$ jet | Number of sampled events |
|---|---|---|---|---|
| 50 | 2 (0.095) | 0 (0) | 0 (0) | 21 |
| 100 | 4 (0.033) | 9 (0.073) | 0 (0) | 123 |
| 300 | 4 (0.069) | 4 (0.069) | 16 (0.276) | 58 |

showers. No close events with separation less than 2500 $\mu$m were found in the chamber C1 of 50-GeV electrons. Only the events confirmed to be initiated by a single electron were analyzed and the number of them in each chamber is given in Table II.

## III. METHOD OF ANALYSIS

*Scanning of emulsion plate.* The general scanning was carried out at one or two layers of each chamber, as summarized in Table II, under a microscope with an object lens of power 20. The tracks of events found in the scanning layer were successively connected to other layers.

Figure 2 shows the depth distribution of layers where the number of shower tracks becomes two or more for the electron-initiated events in each chamber. The dashed histogram is a Monte Carlo simulation result[18] for incident electrons in lead. The experimental data shows a good agreement with the simulation as a whole. In Fig. 3, the distribution of number of shower tracks within radii 50 and 100 $\mu$m for 100-GeV showers at the scanning layers are compared with the simulation. They also show a good agreement with each other. This may demonstrate that our analysis does not take the serious bias in the detection of showers.

*Method of track counting.* First, the shower tracks of all events at every depth were carefully sketched in the data sheets under a microscope with an object lens of power 60 or 40. Then, the shower tracks were counted on each sketch of collected data in several rings with radii up to 100 $\mu$m from the shower axis. By this troublesome method, we are able to measure the position of shower tracks in each plate with a relative error less than 1 $\mu$m.

The angular distribution of shower tracks within radius 100 $\mu$m are shown in Fig. 4 at three depths of the chamber A3 for 300 GeV. The background tracks, which should be attributed to cosmic rays or particles indirectly originated from the accelerator, obtained in interspaces of events is also shown in this figure. The number of the background tracks is negligibly small at every depth except for a few initial layers where the cascade shower did not yet start or just started.

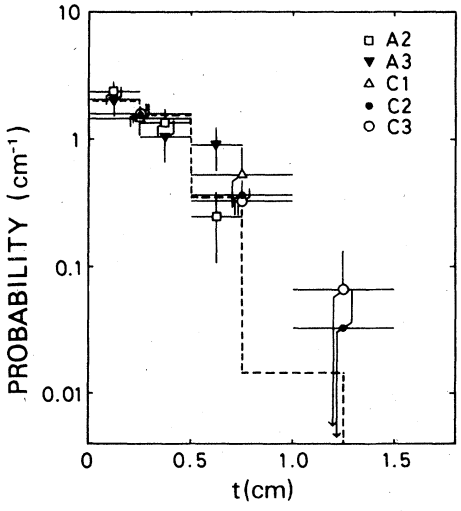


FIG. 2. Distribution of depths where two or more tracks are first found. Dashed histogram is a simulation result.

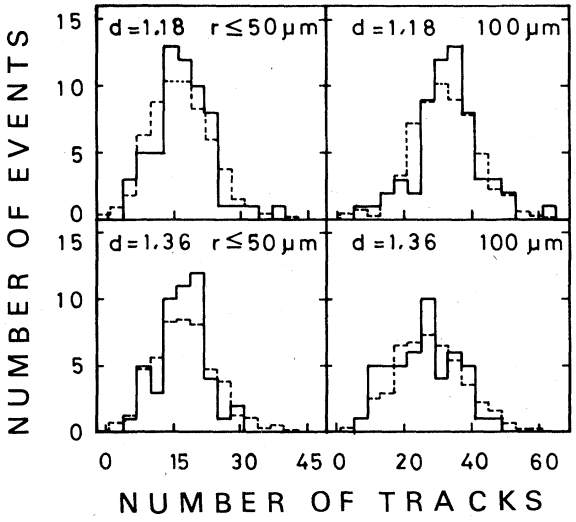


FIG. 3. Comparison of the distribution of number of shower tracks within radii 50 and 100 $\mu$m for 100 GeV (solid histogram) with a simulation (dashed histogram) at the depth of scanning.

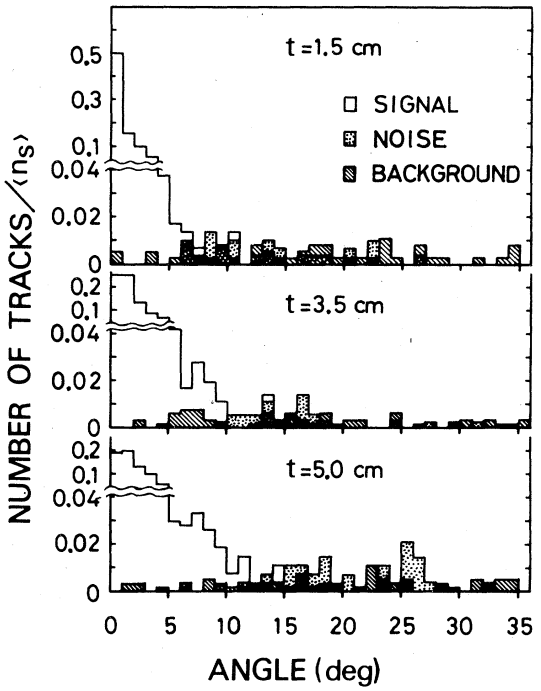


FIG. 4. Angular distribution of shower tracks at depth $t$ of the chamber A3 for 300 GeV. The tracks with angle greater than about 10°, shown by dotted area, are omitted as noise. The background tracks (hatched area) below 10° nearly counterbalance with the resultant noise tracks subtracted by background between 10° and 20°. $\langle n_s \rangle$ means the mean value of number of signal tracks at the depth $t$.

However, the noise tracks at these layers can be easily excluded, because shower tracks, which continue with high energy and are concentrated close to the core, run nearly parallel from the front side to back side of the layers of emulsion plate. In this analysis, also, the large-angle tracks were omitted from the counting, where the cutoff angle was settled to be about 10° to the shower axis as indicated in Fig. 4.

*Location of shower axis.* The shower axis was generally put at a peak of the track density distribution on every layer before and around the depth of shower maximum. According to the simulation,[18] the average error caused by this method is estimated to be ~6 $\mu$m around the shower maximum. After the shower maximum the axis position was chosen so that the number of shower tracks within a radius 50 $\mu$m was largest. To estimate the effect due to the mislocation of shower axis, we tried to give a systematic shift of cascade center with a constant displacement on every target diagram and construct the lateral distribution of shower tracks for each case, as described in Appendix B. From this procedure, the error of axis location is found to be less than 12 $\mu$m in the depth beyond the shower maximum.

## IV. AVERAGE BEHAVIOR OF CASCADE DEVELOPMENT

### A. Longitudinal behavior

The longitudinal development of average number of shower tracks within radii 25, 50, and 100 $\mu$m is shown in Fig. 5. In this figure, the back-side layers of each emulsion plate gives shower tracks (open circles) less than the front-side data (closed

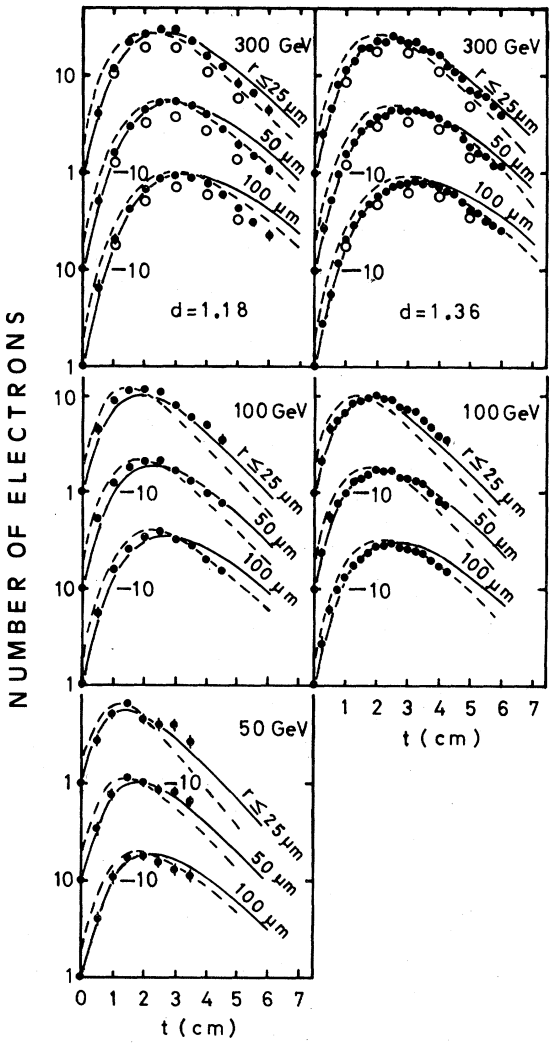


FIG. 5. Longitudinal development of the number of shower tracks within radii 25, 50, and 100 $\mu$m at the front side of emulsion plate (closed circles). The open circles show the back-side data of emulsion plate with 800-$\mu$m-thick acryl base. The solid curves are half of pair curves and the dashed curves are pair curves (see text).

circles) mainly due to the angular divergence in the 800-$\mu$m-thick acryl base. The results are compared with the Nishimura-Kidd calculation in Fig. 5. The dashed curves are the calculation for pair incidence of electrons (pair curve) with just the beam energy in a pair and with the spacing factor 1.18 and 1.36 for type C and A chambers, respectively. The solid curves indicate a half of pair incidence cascade curve (a half of pair curve) with twice the beam energy in a pair. From a simple consideration it is expected that the cascade shower of single-electron incidence should take an intermediate value between the above two curves. In this section, the experimental data is compared mainly with the half of pair curves.

As noticed from the comparison in Fig. 5, the front-side data are in good agreement, independently of incident energies, with the theoretical ones at foregoing layers up to the shower maximum for the respective radii 25, 50, and 100 $\mu$m. After the shower maximum the experimental data shows a somewhat more rapid decrease than the theoretical curves, especially at a large distance from the shower axis. Recently, Nishimura calculated the cascade curve for an electron incidence.[19] If our data are compared with his calculation, a better agreement is obtained, as discussed in Appendix A.

However, we should comment on this apparent agreement between the calculation and data. Namely, the spacing factor[20] does not agree in general with the geometrical dilution factor specified by the chamber construction and its value depends on the location of emulsion layer in a gap between lead plates. That is to say, the Nishimura-Kidd curves do not indicate the number of shower tracks at the front-side layer in contact with the lead plate but at an intermediate depth in the gap.

### B. Lateral behavior

The average lateral distribution of shower tracks at several depths are shown in Fig. 6 for both type A and C chambers. The experimental data are fairly well consistent with the theoretical curves at the preceding layers up to the shower maximum. At the deep layers after the shower maximum the experiment shows slightly smaller densities and steeper slopes than the theory. This behavior is consistent with the rapid decrease noted in the tail of the longitudinal development.

According to the cascade theory under the core approximation[10] the lateral structure function near the shower axis is expressed by a function of $rE_0/K$ and $t$ only, and not of the separate variables of $E_0$ and $r$, where $E_0$ is the primary energy, $r$

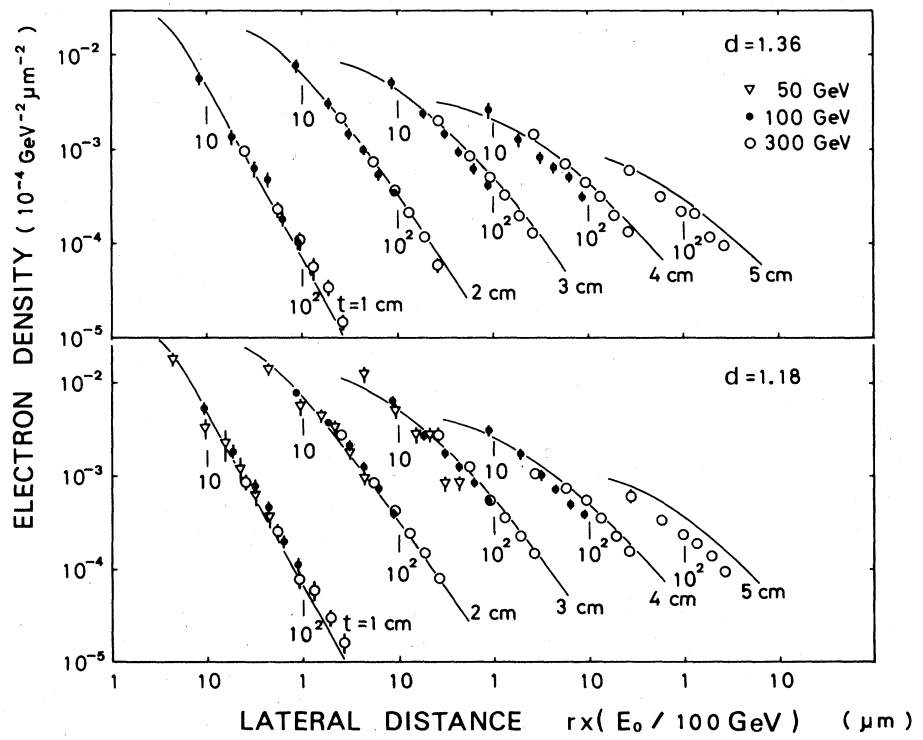


FIG. 6. Lateral distribution of track density. The solid curves are the theoretical ones of a half of pair curve.

the radius, $K$ the scattering constant, and $t$ the depth. This means that if we have obtained the numerical values of the structure function near the shower axis for a shower of a certain primary energy $E_0$, we can predict the one for a shower of a different primary energy. This similarity relation makes it quite simple to perform the actual analysis of the shower phenomena near the shower axis.

The validity of this relation or, in other words, the core approximation is easily examined by comparing data in different primary energies with one another. Figures 7 and 8 show the number of shower tracks within each radius $r = 12.5$, 25, 37.5, 50, 75, and 100 $\mu$m which is plotted against the abscissa $rE_0$ for the type A and C chambers. The experimental data with different initial energies show good consistency with each other at the depth of shower maximum (Fig. 7) and also at the fixed depth of 2 cm of lead (Fig. 8).

However, when the data is taken at greater depths such as 3 and 4 cm, the experimental points begin to shift down in order of energy, from low to high, as the radius increases. Except for these differences the experimental data lie on the theoretical curves. As a result, we can say that the similarity relation keeps its validity within a radius of about 50 $\mu$m at the depth 3 cm for 50 GeV and also it holds within 75 (50) $\mu$m for 100 GeV and within 100 (75) $\mu$m for 300 GeV at the depth 3 (4) cm.

One may notice a discrepancy between the experimental data and the theoretical curve at the small $rE_0$ regions for the 50- and 100-GeV electron incidence especially at greater depths. This discrepancy may come from the error of axis determination described in Sec. III and Appendix B.

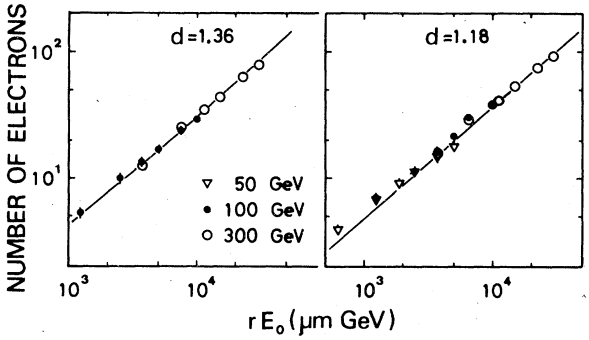


FIG. 7. Similarity relation of the number of shower tracks within a radius $r$ at the depth of shower maximum for respective radius $r$ for 50-, 100-, and 300-GeV showers. The solid curves are the theoretical ones of a half of pair curve.

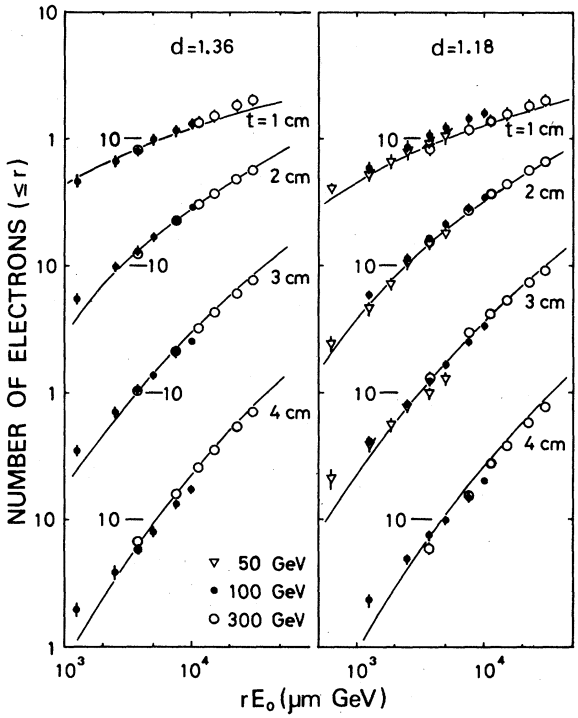


FIG. 8. Same as Fig. 7 at the several depths of lead.

### C. Track length

Figure 9 shows the similarity relation for the track length. In this paper, the track length from the chamber top to a particular depth $t_c$ in lead inside a cylinder of radius $r$ is defined by

$$L(\leq r, t_c) = t_0 \sum_{i=3}^{k} n_i(\leq r) \quad \text{(cm in lead)},$$

where the $t_0$ (= 0.25 cm for the type A chambers, = 0.50 cm for the type C chambers) is the thickness of lead plates $t_c = (k-2)t_0$ and $n_i(\leq r)$ the number of shower tracks within a radius $r$ at the front side of the $i$th emulsion plate from the

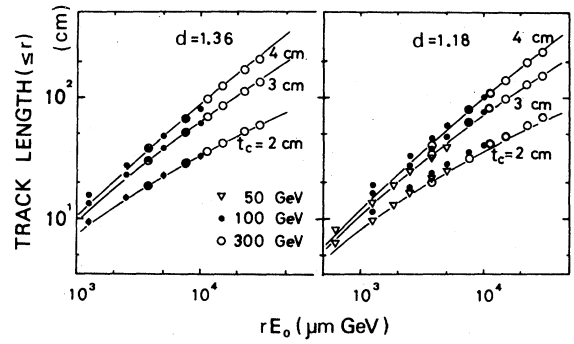


FIG. 9. Similarity relations of track length summed up to the depth $t_c$ within a radius $r$. The solid curves are the theoretical ones of a half of pair curve.

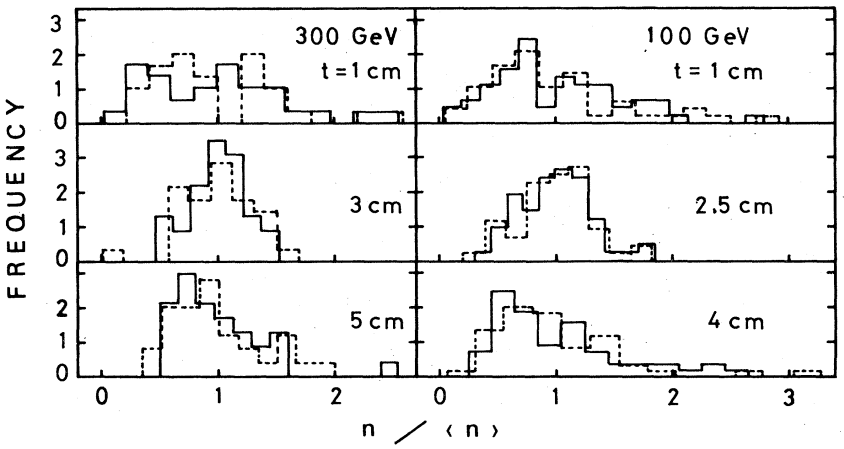


FIG. 10. Number distribution of shower tracks at the several depths within a radius 50 $\mu$m. Solid and dashed histograms are for $d=1.18$ and $d=1.36$, respectively. The areas of the histograms are normalized.

chamber top. The solid curves are obtained from the theoretical curves under the same definition. The experiment also shows a good agreement with the theory as well as in Fig. 7. This is because the number of shower tracks around the shower maximum dominates the track length.

These facts suggest that the number of shower tracks at several layers around the shower maximum and the track length forming them should give a good estimation, at least in an average, of an incident electron energy.

## V. FLUCTUATION OF CASCADE DEVELOPMENT

We obtained the distribution of number of shower tracks, $n(\leq r, t)$, at every depth $t$ of each emulsion chamber. A few examples are shown in Fig. 10 for a disk of radius $r=50$ $\mu$m. The narrowest distribution is given at or around the shower maximum and it tends to expand as the depth varies toward both sides of the shower maximum. The standard deviation of the distribution is plotted in Fig. 11 to show its depth dependence. In

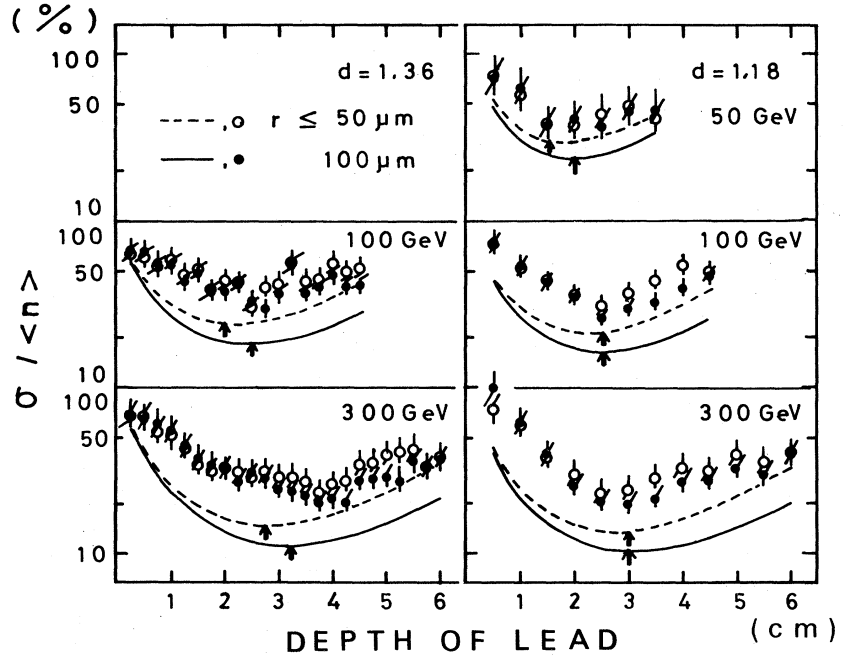


FIG. 11. Depth dependence of the standard deviation $\sigma$ of the number distribution for each circle of radius 50 and 100 $\mu$m. The dashed and solid curves are the expected curves from the Poissonian for radii 50 and 100 $\mu$m, respectively. The arrow indicates the depth of the shower maximum in the average transition curve.

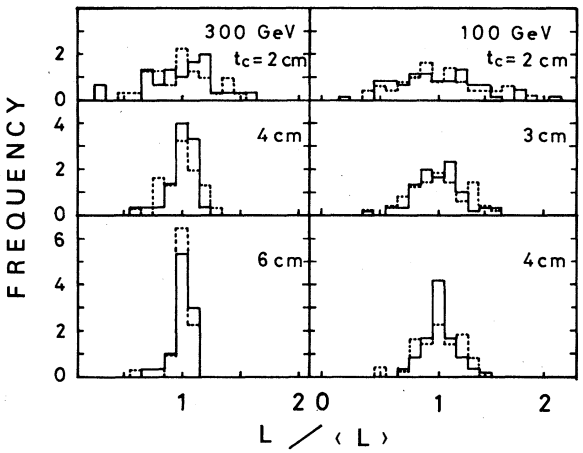


FIG. 12. Track-length distribution up to the several given depths within a radius 50 $\mu$m. Solid and dashed histograms are for $d$=1.18 and $d$=1.36, respectively. The areas of the histograms are normalized.

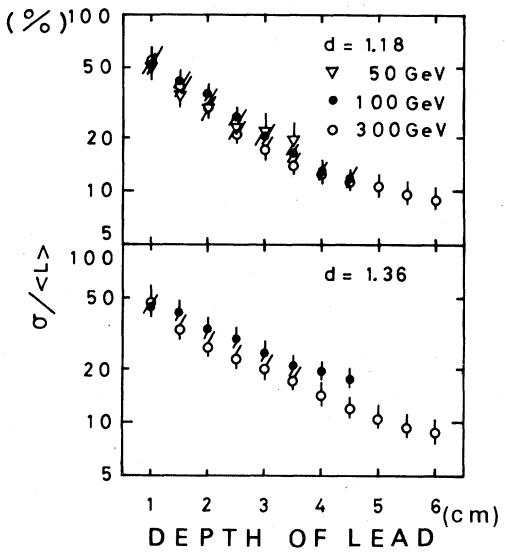


FIG. 13. Depth dependence of the standard deviation $\sigma$ of track-length distribution for the cylinder of radius 50 $\mu$m.

this figure one can notice, in more detail, that the standard deviation decreases with the increasing depth of lead up to the shower maximum and thereafter it increases. At the shower maximum the fluctuation becomes smaller when the initial energy increases. However, the fluctuation is about twice as large as the Poissonian[21] at most depths for every cases.

On the other hand, the distribution width of the track length defined in Sec. IV declines monotonically as the depth of cutting of the tracks increases as shown in Fig. 12 for a cylinder of radius 50 $\mu$m. The standard deviation of the track-length distribution is always less than that of the number distribution except for a few initial layers behind the top lead plates. The dependence of the standard deviation on the sampling depth is shown in Fig. 13 for a cylinder of radius 50 $\mu$m. The small dilution factor ($d$=1.18) gives the slightly faster decrease of the standard deviation than the large one ($d$=1.36).

## VI. RELIABILITY OF ENERGY MEASUREMENTS

In the emulsion-chamber experiment the energy of each cascade shower has been generally estimated by comparing the number of shower tracks within a certain radius with the theoretical transition curves. Now, we try to compare the following three methods actually available for estimating the individual cascade energy.

(a) The maximum number of shower tracks of each shower is compared with the theoretical one.

(b) The data at four layers, each interval being 1 cm lead, centered at the shower maximum of the average transition curve is fitted by the theoretical curves with the method of least squares.

(c) The track lengths from the chamber top to the depths 3.5, 4.5, and 6.0 cm of lead for 50, 100, and 300 GeV, respectively, are compared with the theoretical ones.

A half of pair curve described in Sec. IV is employed as the theoretical one in this comparison. In Tables IV–VI are summarized the mean energy and the standard deviation of the distribution of cascade energies thus estimated for each radii 25, 50, and 100 $\mu$m in three cases. The unreliability of the energy measurement can be expressed by the size of the standard deviation of

TABLE IV. The mean energy $\langle E \rangle$ and standard deviation $\sigma$ of the estimated-energy distribution in case (a) (see text).

| | $d$=1.36 | | | | | | $d$=1.18 | | | | | |
|---|---|---|---|---|---|---|---|---|---|---|---|---|
| | $r \leq 25$ $\mu$m | | ≤50 $\mu$m | | ≤100 $\mu$m | | $r \leq 25$ $\mu$m | | ≤50 $\mu$m | | ≤100 $\mu$m | |
| $E_0$ (GeV) | $\langle E \rangle$ (GeV) | $\sigma$ (%) | $\langle E \rangle$ (GeV) | $\sigma$ (%) | $\langle E \rangle$ (GeV) | $\sigma$ (%) | $\langle E \rangle$ (GeV) | $\sigma$ (%) | $\langle E \rangle$ (GeV) | $\sigma$ (%) | $\langle E \rangle$ (GeV) | $\sigma$ (%) |
| 50 | | | | | | | 75 | 26 | 72 | 30 | 60 | 27 |
| 100 | 175 | 26 | 150 | 27 | 127 | 31 | 163 | 27 | 148 | 23 | 136 | 23 |
| 300 | 417 | 24 | 385 | 21 | 336 | 18 | 413 | 22 | 362 | 19 | 325 | 15 |

TABLE V. Same as Table IV in case (b) (see text).

| | | | $d=1.36$ | | | | | | $d=1.18$ | | | |
|---|---|---|---|---|---|---|---|---|---|---|---|---|
| | $r \leq 25$ μm | | ≤50 μm | | ≤100 μm | | $r \leq 25$ μm | | ≤50 μm | | ≤100 μm | |
| $E_0$ (GeV) | $\langle E \rangle$ (GeV) | $\sigma$ (%) | $\langle E \rangle$ (GeV) | $\sigma$ (%) | $\langle E \rangle$ (GeV) | $\sigma$ (%) | $\langle E \rangle$ (GeV) | $\sigma$ (%) | $\langle E \rangle$ (GeV) | $\sigma$ (%) | $\langle E \rangle$ (GeV) | $\sigma$ (%) |
| 50 | | | | | | | 57 | 27 | 55 | 22 | 46 | 20 |
| 100 | 115 | 29 | 102 | 28 | 90 | 26 | 123 | 23 | 113 | 18 | 99 | 15 |
| 300 | 307 | 19 | 295 | 13 | 276 | 14 | 311 | 14 | 291 | 14 | 270 | 13 |

the obtained energy distribution. On the other hand, the systematic error of the mean energy gives a measure of the validity of using the half of pair curve, although the error mainly originates from the fluctuation of the cascade process in case (a).

The smallest fluctuation is given by case (c), and case (a) gives not only the largest fluctuation but also too high an incident energy on the average. Case (b) is between the above two cases. In every case the fluctuation decreases with increasing initial energy for both the type A and C chambers. However, the type A chambers give a larger fluctuation than the type C chambers with a smaller dilution factor. The lateral dependence of the fluctuation is not significant.

The systematic error in case (c) implies that the half of pair curve gives a slightly larger track length than the experimental data in the region $rE_0 \gtrsim 7500$ μm GeV. In case (b) the estimated mean energy is larger for radius 25 μm or smaller for 100 μm than the given beam energy, i.e., it decreases with the radius. This is corresponding to the steeper lateral distribution in the experiment than that of the half of pair curve. In case (a) also the mean estimated energy decreases with the radius in the same way that the fluctuation at the shower maximum within a certain radius decreases.

When the energy measurement is done within a circle of a radius 50 μm, the unreliability of estimated energy decreases as 28% → 13% in the size of the standard deviation as the incident energy increases as $E_0 = 100 \rightarrow 300$ GeV for $d = 1.36$ and also it decreases as 22% → 14% as $E_0 = 50 \rightarrow 300$ GeV for $d = 1.18$ in case (b). The corresponding values are 27% → 21% and 30% → 19% in case (a), and 18% → 9% and 23% → 9% in case (c). If the systematic error is added to the standard deviation, the total error amounts to about 20–30% for incident energies 100–300 GeV in cases (b) and (c), and about 50–70% in case (a).

## VII. SUMMARY AND DISCUSSION

The experimental result is consistent in a wide view with Nishimura's theory, whose spacing factor is chosen as equal to the dilution factor of the chamber. However, when we look at the data in more details, the following facts or tendencies are noticed.

(1) A very good agreement between the experiment and theory is seen in both the longitudinal and lateral distributions in the region up to the depth at which the average number of shower tracks within a radius 100 μm reaches to the maximum for each incident energy. But after the maximum, the experimental data shows a steep lateral distribution and this leads to somewhat rapid decreases of the transition curves at the large radius.

(2) The similarity relation is completely valid within a radius of at least 100 μm up to the depth of the shower maximum in this radius for the incident energies 50–300 GeV. After the shower maximum the radius in which the relation is valid tends to become small.

(3) The fluctuation of the number of shower

TABLE VI. Same as Table IV in case (c) (see text).

| | | | $d=1.36$ | | | | | | $d=1.18$ | | | |
|---|---|---|---|---|---|---|---|---|---|---|---|---|
| | $r \leq 25$ μm | | ≤50 μm | | ≤100 μm | | $r \leq 25$ μm | | ≤50 μm | | ≤100 μm | |
| $E_0$ (GeV) | $\langle E \rangle$ (GeV) | $\sigma$ (%) | $\langle E \rangle$ (GeV) | $\sigma$ (%) | $\langle E \rangle$ (GeV) | $\sigma$ (%) | $\langle E \rangle$ (GeV) | $\sigma$ (%) | $\langle E \rangle$ (GeV) | $\sigma$ (%) | $\langle E \rangle$ (GeV) | $\sigma$ (%) |
| 50 | | | | | | | 58 | 23 | 61 | 23 | 55 | 25 |
| 100 | 112 | 19 | 100 | 18 | 88 | 20 | 117 | 14 | 107 | 12 | 97 | 14 |
| 300 | 288 | 10 | 280 | 9 | 264 | 10 | 290 | 11 | 278 | 9 | 263 | 8 |

tracks inside a certain radius decreases with the depth up to the shower maximum in that radius and thereafter it increases. It is noticed that the higher the incident energy, the smaller the fluctuation at the shower maximum. But its value is about twice as large as the Poissonian at most depths.

(4) The fluctuation of the distribution of track length, within a certain radius, summed up from the chamber top to a certain depth decreases monotonically with the depth. The slope of the decrease becomes steeper as the dilution factor becomes smaller. The fluctuation is less than that of the number of shower tracks within the same radius at the depth where the tracks are cut except for a few layers behind the top lead plate.

(5) The ambiguity in the energy estimation by the conventional way using the transition curves within a radius 50 $\mu$m decreases as either the incident energy increases or the dilution factor decreases. The standard deviation of the distribution of cascade energy thus estimated is less than 28% for incident electron energy $E_0 \geq 100$ GeV in the case of dilution factor $d=1.36$ and less than 22% for $E_0 \geq 50$ GeV in the case $d=1.18$. In the energy estimation using the track length within the same radius, the standard deviation becomes lower than the above values for $E_0 \geq 100$ GeV when the track length is summed up until the depth $t_c > 1.4$ (or $>1.3$) times the depth of shower maximum in this radius for $d=1.36$ (or $d=1.18$).

It should be noted that the data at the front side of the emulsion plate agree with the theoretical curves having a spacing factor equal to the dilution factor. This means an underestimation of cascade energy, if the dilution factor is employed instead of the spacing factor for a popular-style emulsion chamber in which some materials or x-ray films are inserted between the lead plate and the front surface of the emulsion plate. In such a case it is found, as understood from a difference between the front-side data and back-side data in Fig. 5, that the spacing factor characterizing the theoretical curve has to be chosen somewhat larger than the dilution factor in order to make a good guess of the correct energy.

## ACKNOWLEDGMENTS

The authors would like to express their gratitude to Dr. P. Garbincius, Dr. S. Mori, Dr. B. Cox, Dr. L. Voyvodic, Dr. T. Nash, and Dr. Y. Yamanouchi in Fermilab for making successful exposure of the emulsion chamber to the electron beams. The authors also wish to express their thanks to Professor J. J. Lord and Dr. J. Wilkes at Washington University for offering their facilities necessary for developing the nuclear emulsion plates to us, and Professor J. Nishimura for his useful suggestions. The data were processed with the electronic computer IBM 370/125 in Konan University.

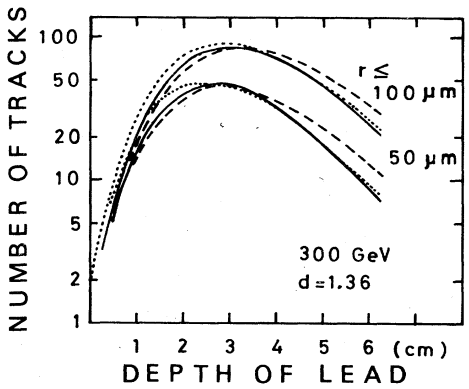


FIG. 14. Comparison of three transition curves, i.e., single electron curve (solid curves), pair curve (dotted curves), and a half of pair curve (dashed curves).

## APPENDIX A

Here, we compare our data with the theoretical transition curve of cascade shower for a single-electron incidence[19] (single-electron curve), which was recently calculated by Nishimura in order to compare with his own experiment.[22]

Figure 14 shows the comparison of this single-electron curve with pair curve and with half of pair curve (see Sec. IV in the text). From a simple consideration it is understood that the single-electron curve should take the intermediate value of the above two curves. They are consistent with each other at depths before the shower maximum, but this single-electron curve gives a smaller value than expected from the other curves at

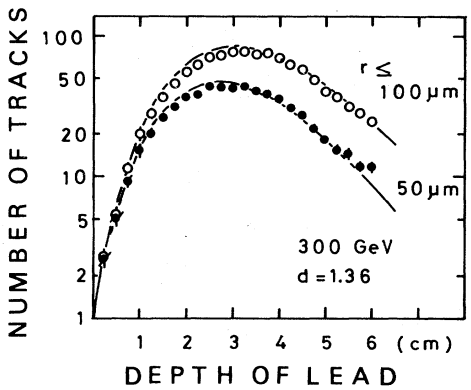


FIG. 15. Comparison of single-electron curve with the experimental data.

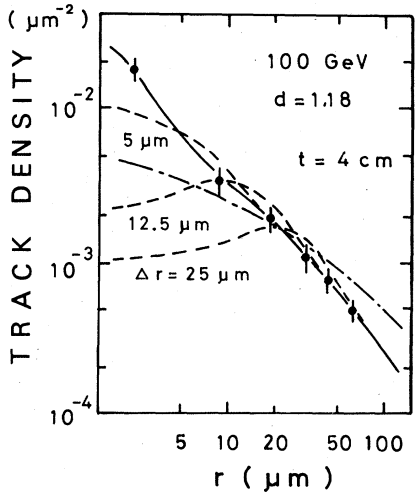


FIG. 16. Differential lateral distribution of the 100 GeV electron incidence in type C chamber at the depth of 4 cm of lead. The solid and dashed curves are respective lateral curves for the experimental data before and after the shift of axis position. $\Delta r$ means the displacement. The dot-dashed curve is the theoretical one of a half of pair curve.

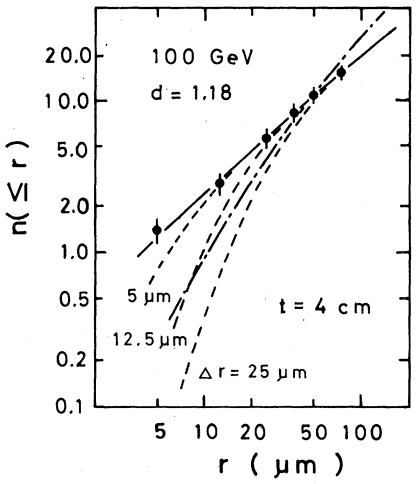


FIG. 17. Integral form of the curves in Fig. 16.

depths after the shower maximum.

As seen in Fig. 15, however, the single-electron curve is in good agreement with the experimental data at layers even after the shower maximum.

## APPENDIX B

In an emulsion-chamber experiment the shower tracks are counted within a circle of a certain radius $r$ from the shower axis. The center of the circle is generally put at a peak of the track density distribution on every layer before and around the depth of shower maximum. After the shower maximum the center is chosen so that the number of shower tracks within a radius $r$ (50 $\mu$m in our case) is largest. In this method a displacement of the center from the real shower axis will be increased with the depth $t$. The error of axis location is essential to a slope of the lateral distribution, especially at a small radius.

To investigate this effect, we try to shift artificially the center in every target diagram with a constant displacement $\Delta r$. Figures 16 and 17 are differential and integral lateral distributions, respectively, for 20 cascade events of 100 GeV incidence in type C chamber at a depth of 4 cm of lead.

Figure 16 shows that the track density becomes smaller near the shower center and also that the slope becomes steeper at the region around $r \approx 2\Delta r$ as the displacement ($\Delta r$) increases. It is a reasonable requirement that the average lateral distribution should generally decrease as the radius increases. Therefore, we can see from Fig. 16 that the experimental error of axis location must be smaller than $\Delta r = 12.5$ $\mu$m. In Fig. 17 there is a difference between the experimental data and the theoretical curves (a half of pair curve described in Sec. IV in the text) at a small radius. This discrepancy is considered to be caused from the above error of axis location. For the systematic displacement $\Delta r = 12.5$ $\mu$m, in practice, the experimental data agrees fairly well with the theory at a small radius. Even though $\Delta r = 12.5$ $\mu$m is the actual uncertainty the experimental point moves only 8% at $r = 25$ $\mu$m, and the effect decreases with the radius.

[1]W. Blockev, R. Kemey, and W. Panofsky, Phys. Rev. 79, 419 (1950).
[2]H. Tom, Phys. Rev. 136B, 447 (1964).
[3]H. Lengeler, W. Tejessy, and M. Deutschmann, Z. Phys. 175, 283 (1963); Nuovo Cimento 28, 1501 (1963).
[4]D. I. Sober *et al.*, Nucl. Instrum. Methods 109, 29 (1973).
[5]D. Muller, Phys. Rev. 5, 2677 (1972).
[6]C. J. Crannell, Phys. Rev. 161, 310 (1967).
[7]T. Yuda *et al.*, Nuovo Cimento 65A, 205 (1970); Nucl. Instrum. Methods 73, 301 (1969).
[8]W. R. Nelson *et al.*, Phys. Rev. 149, 201 (1966).
[9]B. Rossi and K. Greisen, Rev. Mod. Phys. 13, 240 (1941).
[10]J. Nishimura, *Encyclopedia of Physics*, edited by S. Flugge (Springer, Berlin, 1967), Vol. XLVI/2, p. 1ff.
[11]For example, H. Messel and D. F. Crawford, *Elec-*

*tron-Photon Shower Distribution Function* (Pergamon, New York, 1970).
[12]ICEF Collaboration, Nuovo Cimento Suppl. 1, 1039 (1963).
[13]M. Akashi *et al.*, Prog. Theor. Phys. Suppl. 32, 1 (1964).
[14]J. Kidd and J. Nishimura, Nuovo Cimento Suppl. 1, 1086 (1963).
[15]O. Minakawa *et al.*, Nuovo Cimento Suppl. 11, 125 (1958); Japan-Brazil emulsion collaboration, CKJ Report No. 13, Cosmic Ray Laboratory, University of Tokyo, 1974 (unpublished).
[16]J. Nishimura, using K. Pinkau's data [Philos. Mag. 2, 1389 (1957)], showed this consistency in Ref. 10.
[17]C. Halliwell *et al.*, Nucl. Instrum. Methods 102, 51 (1972).
[18]K. Kasahara (private communication).
[19]J. Nishimura (private communication).
[20]J. Nishimura, Prog. Theor. Phys. Suppl. 32, 72 (1964).
[21]L. Janossy and H. Messel, Proc. Phys. Soc. London 63A, 1101 (1950).
[22]J. Nishimura *et al.*, Astrophys. J. (to be published).